Intermetallics 40 (2013) 65–70

Contents lists available at SciVerse ScienceDirect

Intermetallics

journal homepage: www.elsevier.com/locate/intermet

The effect of heat treatment on crack control and grain refinement in laser beam welded β-solidifying TiAl-based alloy

J. Liu [a,b,*], M. Dahmen [b], V. Ventzke [a], N. Kashaev [a], R. Poprawe [b]

[a] Helmholtz-Zentrum Geesthacht, Institute of Materials Research, Max-Planck-Straße 1, 21502 Geesthacht, Germany
[b] Fraunhofer Institute for Laser Technology (ILT), Steinbachstraße 15, 52074 Aachen, Germany

ARTICLE INFO

Article history:
Received 20 November 2012
Received in revised form
10 April 2013
Accepted 11 April 2013
Available online 12 May 2013

Keywords:
A. Titanium aluminides, based on TiAl
B. Phase transformation
C. Laser processing
D. Microstructure

ABSTRACT

Investigations were conducted on the γ-TiAl-based alloy Ti–42Al–2.5Cr–1Nb–0.7Si–0.5B (at. %) to assess the influence of in situ and conventional post-weld heat treatment on the microstructure and microtexture transformations induced by laser beam welding. It was found that in situ post-weld heat treatment at 800 °C was important to inhibit weld seam cracking. EBSD and HEXRD results indicated that the welding zone mainly consisted of coarse α_2 "textured colonies". These textured α_2 are found to be in Burgers orientation relationship with their parent β grains. After 1 h of conventional post-weld heat treatment at 1200 °C followed by furnace cooling, the textured colonies are refined. The α_2 grains nucleate heterogeneously on borides so that the sharp texture of the weld zone was broken down.

1. Introduction

Intermetallic alloys based on γ-TiAl are attractive candidates for innovative thermal and mechanical applications due to their low densities, good high-temperature tensile properties and excellent creep and oxidation resistance [1–13]. They have great potential to replace nickel-based alloys intended for service at temperatures up to 800 °C [1,3,9]. Diffusion bonding, infrared brazing, laser beam and electron beam welding have been investigated with the aim of producing sound TiAl joints [5,7,8,14–16]. However, due to the limited ductility and damage tolerance at room temperature, the γ-TiAl-based alloys have been reported as having limited weldability. Butt joints are reported to be only available of small pieces [5]. The deficiencies are associated not only with intrinsic brittleness of the material but also with the high amount of residual stress that is generated by welding thermal cycle. Due to the intrinsic brittleness of the material at low temperature, cracks along the longitudinal and/or transverse directions have often been observed in weld seams. One possible solution for crack elimination is pre- and post-heating the base metal with a pre-heated ceramic heat insulator underlay. This method was shown to reduce the probability of cracking on work pieces around 60 mm in length [7]. A high amount of residual stress, which results in crack initiation and propagation, has been reported in laser joint plates [8]. In situ post-weld heat treatment with a secondary defocused laser beam has been used to reheat the welded seam immediately after welding, which reduced the maximum value of the longitudinal stress from over 1000 MPa to less than 500 MPa [16]. Moreover, embrittlement could also be caused by absorption of oxygen into the surface region, which gives rise to a significant tensile stress in the sample [17].

Not only should the welded TiAl-based alloys be crack-free, but also the microstructure needs to be optimised in the weld zone. Laser beam welded TiAl-based alloys typically consists of large amount of brittle α_2 phase. Thus great emphases have been placed on microstructural refinement to improve the ductility of the material. Hecht [18] and Hu [19] have shown the refinement through heterogeneous nucleation of α on borides during β/α transformation. The mechanism was first explained by Cheng [20], the borides cause strong constitutional undercooling in the segregation zone due to the pronounced partitioning of boron, and lead to lots of nucleation sites in the interdendritic spaces during solidification. A convoluted microstructure was generated in IRC, Birmingham. The material was quenched to massive γ and differently orientated γ plates which precipitated in a heavily faulted γ matrix [21]. Clemens [13] also refined the grains of the material through cycle heat treatments. The presence of quenching stress could play an important role in triggering the recrystallisation of α at 900 °C. A recent study by Oehring et al. [22] also indicates that grain refinement through borides depends strongly on the cooling rate

* Corresponding author. Helmholtz-Zentrum Geesthacht, Institute of Materials Research, Max-Planck-Straße 1, 21502 Geesthacht, Germany. Tel.: +49 4152 87 2563; fax: +49 4152 87 2534.
E-mail address: jie.liu@hzg.de (J. Liu).

0966-9795/$ – see front matter © 2013 Elsevier Ltd. All rights reserved.
http://dx.doi.org/10.1016/j.intermet.2013.04.007

from the β phase. The heterogeneous nucleation of α on boride could be suppressed by high cooling rates.

The production of joints with homogeneous fine-grained microstructure, without cracking and significant texture is of great importance for the application of TiAl-based alloys. The present work is devoted to the production of sound welding seams. Microstructure, microtexture and high-energy X-ray diffraction (HEXRD) investigations have been carried out towards the development of appropriate welding procedures.

2. Experimental procedures

The alloy under investigation has the composition Ti–42Al–2.5Cr–1Nb–0.7Si–0.5B (at. %). The actual composition was verified by energy dispersive spectroscopy (EDS) and was found to be within 1% of the nominal value. The base material was cast, HIPed and sectioned by electro-discharge machining into pieces of 13 mm × 25 mm × 2.7 mm. Sample surfaces were cleaned and ground with 2000 #grit SiC paper to remove oxides and machining remnants. The experimental set-up includes a CO_2 laser, an induction furnace and an oxygen measuring facility. A robot was used to control the laser beam movement in the *x-y-z* coordinate system. The welding plates were heated by an induction furnace, which was filled with argon to protect the plates from oxidation. The residual oxygen content in the welding chamber was continuously measured, and each welding process was carried out after the oxygen content was below 100 ppm. Helium was used as the assist gas supplied by an off-axis nozzle to the weld zone. Specimen temperature was measured using K-type thermocouples which were arc welded onto the heat-affected zone (HAZ), the data was continuously recorded.

The welding process was divided into three steps: pre-heating, welding and post-weld heat treatment. All plates were pre-heated by induction to 600 °C and then held for 1 min to establish temperature homogeneity throughout the whole sample. The welding process was carried out with a laser beam power of 1200 W at the workpiece at a feed rate of 1.5 m/min. In situ post-weld heat treatment at temperatures of 25 °C (sample #1), 400 °C (sample #2) and 800 °C (sample #3) for 1 min was carried out by induction heating immediately after welding. After post-weld heating, the samples were air-cooled. A fourth welded specimen (sample #4) was made using the same procedure as sample #3, was conventionally heat treated at 1200 °C for 1 h in a vacuum furnace and then furnace cooled.

The welds were visually inspected and investigated by radiography to detect cracks and porosity. The as-welded specimens were sectioned, ground and polished, and finally mechanically polished with a vibrating polisher. The microstructure was examined using Scanning Electron Microscopy (SEM) in backscattered electron (BSE) mode in a Zeiss DSM962 and a LEO Gemini 1530 microscope equipped with EDS, electron backscatter diffraction (EBSD) and the associated data analysis systems. HEXRD experiments using synchrotron radiation were performed at the HZG beamline HEMS (High Energy Materials Science) at Deutsches Elektronen-Synchrotron (DESY), Hamburg. HEXRD experiments were conducted in transmission at room temperature on the same specimen slices that had been used for microstructural analysis. The incident beam had a photon energy of 87.1 keV with a cross-section of 1 mm × 1 mm. The detector was orientated strictly perpendicular to the incident beam. The diffraction patterns were recorded and the microstructure of the material was analysed.

3. Results and discussion

Cracks transverse to weld seam can be observed in specimens #1 and #2 (Fig. 1(a)). When the specimens were in situ post-weld heat treated at 800 °C, a sound square butt weld was produced. As shown in Fig. 1(b)–(d), the joint is free of pores and macro cracks, and both upper and lower beads of the weld seam show a bright metallic surface. Hence a take-up of oxygen can be excluded. By comparison of various in situ post-weld heating temperatures from specimens #1 to #3, it is discovered that in situ post-weld heating temperature plays an important role in avoiding the formation of cracks. Cracking can be eliminated when the specimen is in situ post-heated at 800 °C. When the weld zone is in situ post-heat treated above the brittle-to-ductile transition temperature, the material in the weld zone undergoes phase transformation and deformation assisted by dislocation motion. Thus, the tendency for cracking can be dramatically reduced [21]. However, the in situ heating at lower temperatures, such as 25 °C and 400 °C, are not sufficient to inhibit cracking.

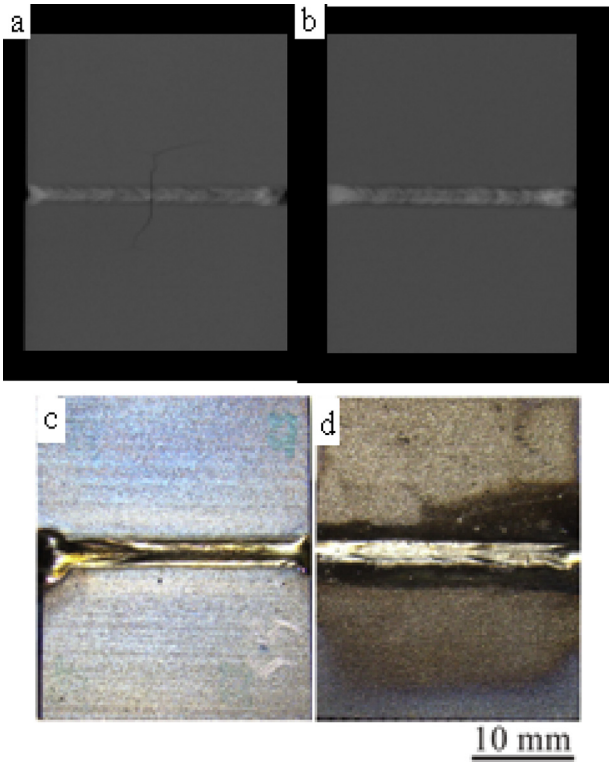

Fig. 1. (a) Representative radiograph of specimen #1; (b) radiograph of crack-free specimen #3, upper (c) and bottom (d) sides of specimen #3.

According to the binary phase diagram [23], the titanium aluminide alloys can solidify completely through the β phase for Al concentrations up to around 44 at% Al. Both Nb and Cr are recognised as β stabilizers, as their effect is shifting the α/β primary-solidification phase boundary to higher aluminium content [24]. The alloy Ti–42Al–2.5Cr–1Nb–0.7Si–0.5B, contains the β stabilizing alloying elements Cr and Nb, which combined with the low Al content. Thus the β phase is the only metallic phase present immediately after solidification is complete and this alloy can be recognised as a β solidifying alloy.

Fig. 2(a) shows the microstructure of the base material stemming from the solidification path $L \rightarrow L+\beta \rightarrow \beta \rightarrow \beta+\alpha \rightarrow +\beta+\alpha+\gamma \rightarrow B2+\alpha_2+\gamma$. The γ-TiAl is coloured dark grey, the α_2-Ti_3Al is light grey, and B2 appears as the brightest phase. The B2 is found to be enriched in Cr, Si and Nb and depleted in Al, its composition determined by EDS was Ti–31.98Al–2.95Cr–1.2Nb–1.05Si. The B2 phase is mainly located along colony boundaries and sometimes within the colony interior. It does not form a complete layer around the lamellar colonies but is

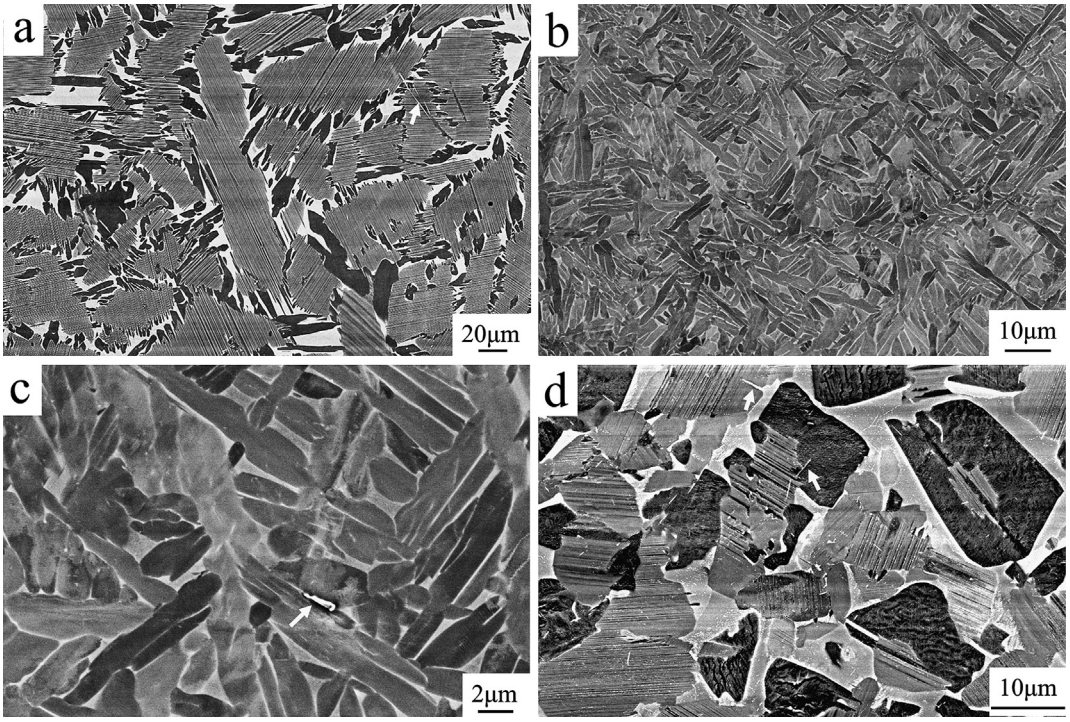

Fig. 2. SEM images taken in back scattered electron (BSE) mode of microstructure of (a) base material, weld zone with low (b) and high (c) magnification and (d) weld zone after annealing.

intersected by small γ grains. Most of the γ grains stem from γ lamellae in the colony and grow into the β region. Cheng et al. [25] found out that these coarsened γ grains have the same orientation with their thinner lamellar counterparts. The borides, indicated by arrows, are in the long straight ribbons or a blocky morphology across the colony boundaries. These borides are reported to play an important role in grain refinement through heterogeneous nucleation of α [18,19,26]. The volume fraction of the three phases in the base material, determined by EBSD, is 18.2% B2, 17.6% α_2 and 64.3% γ. The lamellar (γ + α_2) colonies have an average diameter of approximately 100 μm.

The weld zone (Fig. 2(b)) is composed of fine acicular α_2 plates distributed with different orientations, and average dimensions of about 8 μm length and 2 μm width. The fine acicular α_2 plates in weld zone are separated by bright layers, which are enriched in Nb and Cr. Niobium was expelled into the α grain boundaries during the transformation from β to α_2. Due to the high cooling rate between solidification and 800 °C, chemical homogenization is not attained and this gives rise to the bright ridges [19]. It is not easy to identify borides under the microscope (Fig. 2(b)), only one rod-shaped boride was found lying along the α_2 colony boundary (Fig. 2(c)). After welding, the volume fraction of α_2 phase is significantly increased to 92.1%, which is five times more than that of the base material. Accordingly, the volume fractions of the B2 and γ phases decreased to 4.1% and 3.8%, respectively.

In order to reduce the amount of brittle α_2 phase in the weld zone, a conventional heat treatment for 1 h at 1200 °C was carried out on specimen #4. The weld zone microstructure (Fig. 2(d)) changes to γ, B2 and lamellae. After this heat treatment there is a greater number of borides than in the untreated weld zone and they are found solely in γ or lamellae, or at the boundary of γ and lamellae grains. The γ grains are intersected by B2 as a result of direct nucleation or discontinuous coarsening of B2 via B2 [25]. The volume fraction of B2 and γ increases significantly after heating for 1 h at 1200 °C, and the phase fractions change to 10% B2, 53% α_2 and 37% (in vol. %).

According to Gey and Humbert [27] the misorientation angles between α laths originating from the same β grain can only be 10.5°, 60°, 60.8° and 90°. Thus, the misorientation angle can be applied to determine whether α grains obey the Burgers relationship with respect to the parent β grains. From the α_2 phase texture map in the base material (Fig. 3(a)), the material consists of coarse equiaxed α_2 grains. The misorientation angles (Fig. 3(b)) show peaks slightly preferred in the range of 8–12°. This indicates that the borides lead to grain refinement in the base material during the solidification and most of the α grains are non-Burgers.

The texture map of the α_2 phase in the weld zone (Fig. 4(a)) indicates that a large number of fine α_2 plates have the same orientation as the neighbouring grains, this is indicated by a large pink area at the top and central part of the map. (For interpretation of the references to colour in this figure, the reader is referred to the web version of this article.) A similar result was also found for Fig. 6(a) and (c) in Ref. [18]. Although the colonies of the plates are separated by the bright ridges, these colonies present to be of the same orientation in the top, middle and bottom part of the figure. As a result of this effect, the colony size in the weld zone cannot be simply identified by the dimension of the α_2 plates, rather than dependent on the size of the "textured colonies". The coarsened "textured colonies" could depress the refinement by the thin α_2 plates as presented by the microstructure. The pole figure (Fig. 4(b)) indicates a rather random orientation distribution of the α_2 phase base plane, this results in a broad distribution of misorientation angles (Fig. 4(c)), and there is little preference for the angles 8–12°, 58–62° and 88–92°. The broad distribution of misorientation angles can be due to α_2 plates from different β dendrites and α_2 grains next to the beta grain boundary. There are three possibilities for the formation of the texture map (Fig. 4(a)). Firstly, the α grains nucleate heterogeneously on borides, through the various orientation relationships indicated as $(0001)_\alpha//(001)_{B27}$ and $\langle 11\bar{2}0\rangle_\alpha//[010]_{B27}$ by Hu [19], or by Genç $[01\bar{1}1]_\alpha//[\bar{1}04]_{B27}$, $[2\bar{1}\bar{1}0]_\alpha//[010]_{B27}$ [28] as well as by Banerjee $(1\bar{1}01)_\alpha//(001)_{B27}$, $(11\bar{2}0)_\alpha//(010)_{B27}$ and $(1\bar{1}0\bar{2})_\alpha//(100)_{B27}$ [29]. As a result of

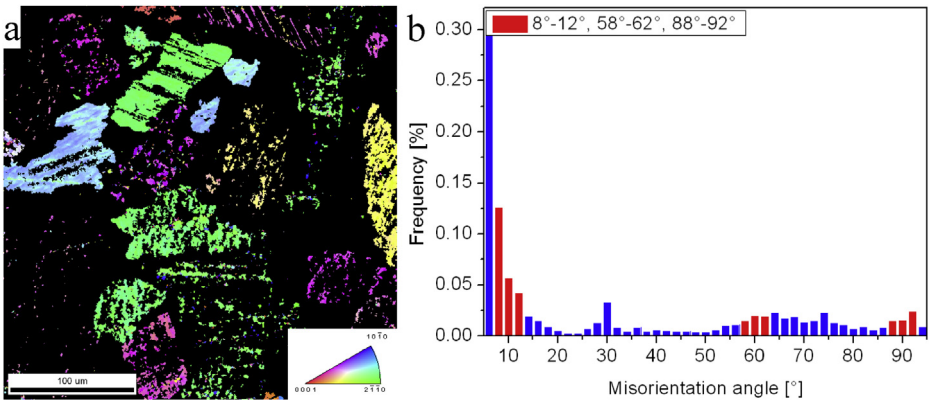

Fig. 3. EBSD measurements of Ti_3Al phase in the base material (a) texture map and (b) misorientation angle between neighbouring Ti_3Al grains.

different orientations from boride nucleation sites, a large number of α grain orientations could be generated. Secondly, the α grains follow the Burgers orientation relationship from their primary β grains. When the α grains are generated from several overlapping β grains, the final misorientation angle depend largely on the misorientation of different parent β grains. The interaction of several overlapping β dendrites could lead to a broad misorientation distribution between α_2 grains. Thirdly, the borides nucleate from β through $\{011\}_{\beta}//(001)_{B27}$ and $<111>_{\beta}//[010]_{B27}$. At the same time, the α_2 phase heterogeneously nucleates on boride with the orientation relationship of $(0001)_{\alpha}//(001)_{B27}$ and $\langle 11\bar{2}0\rangle_{\alpha}//[010]_{B27}$, as observed by Hill et al. [30] and Hu et al. [19,26]. The nucleation of boride on β

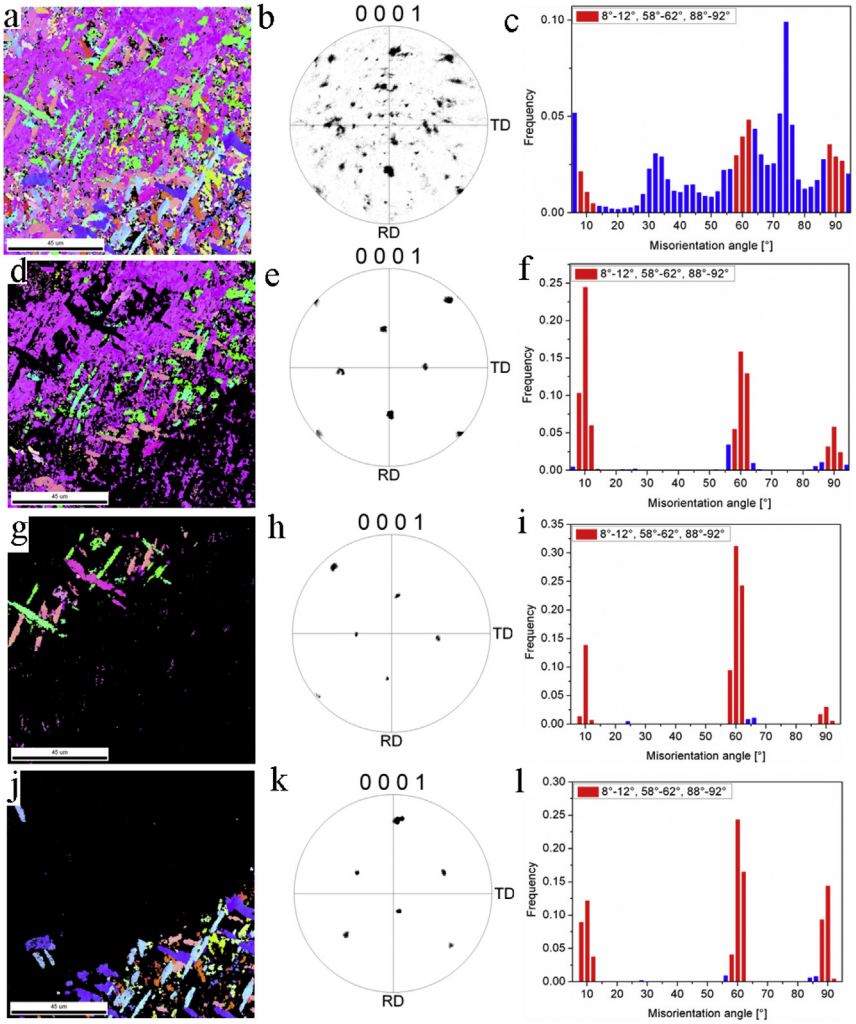

Fig. 4. EBSD measurements of Ti_3Al phase in the as-welded weld zone (a) texture map of all Ti_3Al phase, (b) pole figure of all Ti_3Al phase, (c) misorientation angle between neighbouring grains, (d), (g) and (j) texture map of three groups of Ti_3Al grains, (e), (h) and (k) show the corresponding pole figures of the three grain groups, (f), (i) and (l) misorientation angle between neighbouring Ti_3Al grains of the three grain groups.

phase followed by nucleation of the α_2 phase on boride with the restricted orientation relationship listed above can lead to the formation of Burgers α_2. In order to verify the three hypotheses listed above, the original pole figure and texture map of α_2 grains were divided into different parts as shown in Fig. 4(d)–(l). It is interesting to observe that the pole figures, i.e. (e), (h) and (k), consist of points with misorientation angles of 60° or 90°. In Fig. 4 (e), the position of the {0001} poles of the grains in the area of mapping actually corresponds well to {110} poles of a β grain aligned with the [100] crystal direction parallel to the direction of TD. Fig. 4(h) and (k) shows the same correspondence between $\{0001\}_\alpha$ and $\{110\}_\beta$, even though the primary β is rotated to some degrees. The misorientation angle of three groups of α_2 grains is shown in Fig. 4(f), (i) and (l). All these figures show high intensity at angles of 8–12°, 58–62° and 88–92° for three separated grain groups. This proves that each group of α grains follow the Burgers orientation relationship in the weld zone.

The amount of α_2 phase was significantly reduced after the specimen was heat treated at 1200 °C for 1 h followed by furnace cooling (Fig. 5). The α_2 laths are reformed into an equiaxed morphology in the heat-treated weld zone. The misorientation angle figure (Fig. 5(c)) shows peaks at angles of 8–12°, 58–62° and 88–92°, indicating that a small number of the equiaxed α_2 grains originated from the same primary β. Only two groups of Burgers α grains are found in the texture map (Fig. 5(d)–(i)), around 35% of α grains are textured. Compared with the coarsened textured colonies in Fig. 4(d), the α_2 phase forms independent grains with their individual orientation. The reduced number and size of the textured colonies in the weld zone due to heat treatment lead to the conclusion that the colony size is actually refined.

Although the EBSD provides information about texture, it is restricted to the surface region. In order to examine the grain distribution in a large volume, HEXRD experiments were performed in transmission mode on the same slice of material that had been used for EBSD analysis. The beam was arranged to measure the separate positions of weld zone and base material. The beam interaction measurement volume was 1 mm × 1 mm × 2.7 mm. The Debye–Scherrerr diffraction rings were recorded by a Perkin–Elmer detector. The diffraction rings were unrolled to lines and powder diffractograms were calculated by azimuthally integrating patterns over 360°. The wavelength of the incident beam was 0.14235 Å. As shown in Fig. 6(a) and (b), the $(110)_\beta$ and $(002)_{\alpha 2}$ present several single points rather than a continuous line, indicating that the base material and the weld zone material consist of coarse grains or coarse grain colonies, which is consistent with the results shown earlier. Comparatively speaking, the diffraction line of $(110)_\beta$ and $(002)_{\alpha 2}$ in Fig. 6(c) demonstrates that the grains in the annealed weld zone are refined. As marked by the solid ellipse, the diffraction twins indicate that the (110) of β is parallel to the base plane of α_2. The parallel twins of β and α_2 correspond almost perfectly in Fig. 6(b). However, $(110)_\beta$ and $(002)_{\alpha 2}$ do not correspond very well in Fig. 6(a). It can be deduced that in the cast base material, the prevailing α nucleate heterogeneously through borides while only a minority of α grains nucleate at the grain boundary of the primary β grains.

Thus although it seems as the microstructure was refined by α nucleation on boride in the cast specimen, this refinement could be hampered by any heat treatment. The α_2 and β grains present Burgers orientation relationship after laser beam welding followed by air cooling (Fig. 6(b)). At the same time, the β grains tend to grow along more than one direction in the melt pool of the weld zone, and several β grains could overlap each other. The textured colonies in the weld zone were refined after heated up to 1200 °C followed by furnace cooling. The heterogeneous nucleation of α on borides plays an important role during furnace cooling, because the α_2 and

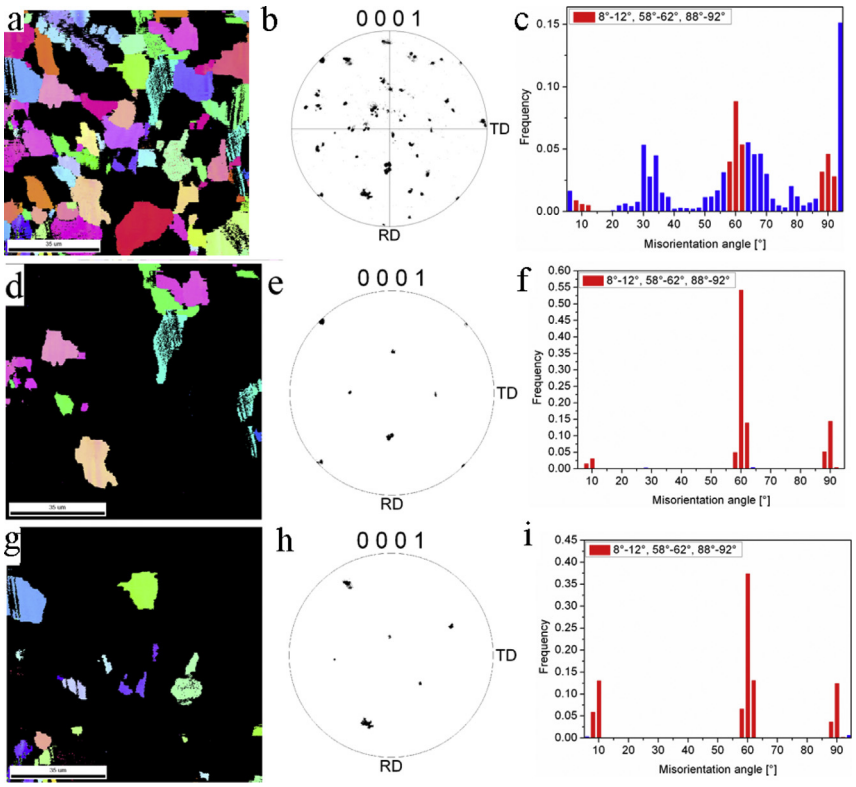

Fig. 5. EBSD measurements of Ti_3Al phase in the annealed weld zone (a) texture map of all Ti_3Al phase, (b) pole figure of all Ti_3Al phase, (c) misorientation angle between neighbouring grains, (d) and (g) texture map of two groups of Ti_3Al grains, (e) and (h) show the corresponding pole figures of two grain groups, (f) and (i) misorientation angle between neighbouring Ti_3Al grains of two grain groups.

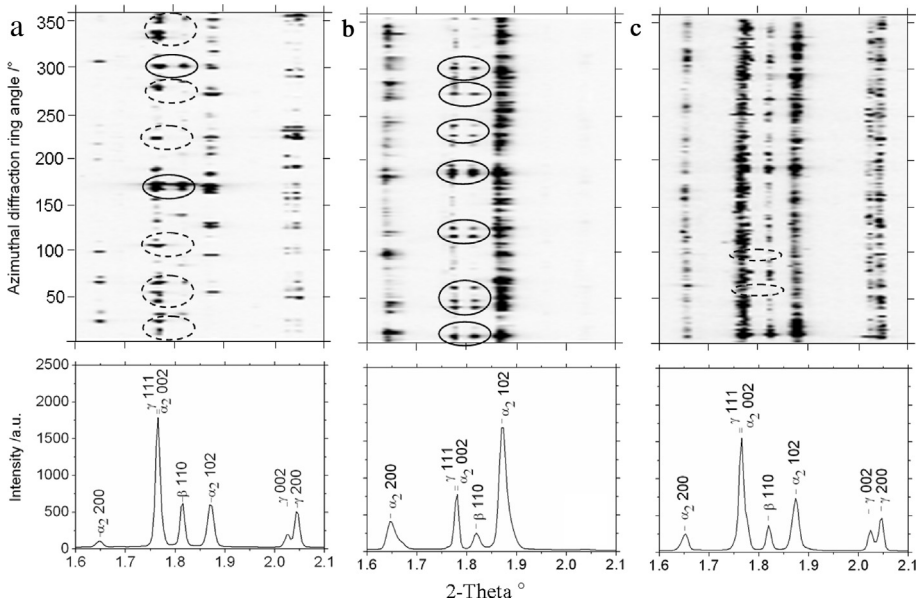

Fig. 6. X-ray diffraction patterns of the (a) base material, (b) as-welded weld zone, (c) annealed weld zone. The Debye–Scherrer diffraction rings have been unrolled to lines as well as azimuthally integrated. The solid and the dashed ellipses indicate reflection pairs that correspond and do not correspond to the Burgers orientation relationship, respectively.

β diffraction line also shows non-corresponding patterns, as indicated by dashed ellipse in Fig. 6(c), and less Burgers α are found in annealed weld zone.

It has been found out that coarse textured α colonies form as a result of high cooling gradient during the laser beam welding process, which for the first time is reported here. This result is in agreement to the conclusion drawn by Oehring et al. [22], who found out that grain refinement mechanism was strongly dependent on cooling rate. The α grains would form coarsened textured colonies when the cooling rate is high in the weld zone, as shown in Figs. 4 and 6(b). The nucleation mechanism for the formation of Burgers α_2 variants remains unknown. The α_2 grains could be nucleated either from their primary β grains or from borides. In the latter case any orientation relationships between β and borides, and between borides and α_2 should meet strict requirements.

4. Conclusions

The study investigated the effect of post-weld heat treatment on the microstructure and texture of the TiAl-based alloy Ti–42Al–2.5Cr–1Nb–0.7Si–0.5B. The following conclusions can be made.

1. The in situ post-weld heat treatment has a positive effect on reducing cracking in the weld zone produced by laser beam welding. Cracking was eliminated by in situ post-weld heating at 800 °C for 1 min. In situ post-weld heating at lower temperatures was not sufficient to produce crack-free welds.
2. A large amount of α_2 phase is formed at high cooling gradient after laser beam welding. The weld zone consists of very coarse "textured α_2 colonies" with a sharp texture. The EBSD and HEXRD analysis have shown that, after laser beam welding followed by air cooling until 800 °C, these "textured α_2 grains" are in Burgers orientation relationship with the parent β grain. The effect of grain refinement by boride was suppressed by the coarse textured colonies at high cooling rate. The nucleation mechanism of the Burgers α_2 variants remains unknown.
3. With conventional post-weld annealing at 1200 °C for 1 h leads to the decomposition of α_2 grains in the weld zone. Grain refinement occurs as a consequence of heterogeneous nucleation of α on boride also plays an important role in grain refinement for low cooling rates.

Acknowledgements

The authors thank the kind discussions from Dr. Michael Oehring, Dr. Jonathan Paul, Dr. Andreas Stark and Prof. Florian Pyczak and support from Dr. Peter Staron and Dr. Norbert Schell in the synchrotron measurement from Helmholtz-Zentrum Geesthacht.

References

[1] Clemens H, Kestler H. Adv Eng Mater 2000;2:551–70.
[2] Sauthoff G. Intermetallics. 1st ed. Weinheim: WILEY-VCH; 1995.
[3] Appel F, Paul JDH, Oehring M. Gamma titanium aluminide alloys acience and technology. Weinheim: WILEY-VCH; 2011.
[4] Leyens C, Peters M. Titanium and titanium alloys. Weinheim: WILEY-VCH; 2003.
[5] Chaturvedi MC, Xu Q, Richards NL. J Mater Process Technol 2001;118:74–8.
[6] Hu D, Botten RR. Intermetallics 2002;10:701–15.
[7] Chen GQ, Zhang BG, Liu W, Feng JC. Intermetallics 2011;19:1857–63.
[8] Liu J, Ventzke V, Staron P, Brokmeier H-G, Oehring M, Kashaev N, et al., editors. Materials processing and interfaces. Supplemental proceedings, vol. 1. Warrendale (PA): TMS; 2012. p. 887–94.
[9] Noda T. Intermetallics 1998;6:709–13.
[10] Imayev RM, Imayev VM, Oehring M, Appel F. Intermetallics 2007;15:451–60.
[11] Liu ZC, Lin JP, Li SJ, Chen GL. Intermetallics 2002;10:653–9.
[12] Chen GL, Sun ZQ, Zhou X. Mater Sci Eng A 1992;153:597–601.
[13] Clemens H, Bartels A, Bystrzanowski S, Chladil H, Leitner H, Dehm G, et al. Intermetallics 2006;14:1380–5.
[14] Glatz W, Clemens H. Intermetallics 1997;5:415–23.
[15] Shiue RK, Wu SK, Chen SY. Intermetallics 2004;12:929–36.
[16] Liu J, Ventzke V, Staron P, Schell N, Kashaev N, Huber N. Adv Eng Mater 2012;14:923–7.
[17] Wu X, Huang A, Hu D, Loretto MH. Intermetallics 2009;17:540–52.
[18] Hecht U, Witusiewicz V, Drevermann A, Zolliner J. Intermetallics 2008;16:969–78.
[19] Hu D, Yang C, Huang A, Dixon M, Hecht U. Intermetallics 2012;23:49–56.
[20] Cheng TT. Intermetallics 2000;8:29–37.
[21] Wu X, Hu D. Scr Mater 2005;52:731–4.
[22] Oehring M, Stark A, Paul JDH, Lippmann T, Pyczak F. Intermetallics 2013;32:12–20.
[23] Witusiewicz VT, Bondar AA, Hecht U, Rex S, Ya Velikanova T. J Alloys Compd 2008;465:64–77.
[24] Inui H, Johnson DR, Yamaguchi M. Mater Sci Forum 2003;426-432:1733–8.
[25] Cheng TT, Loretto MH. Acta Mater 1998;46:4801–19.
[26] Hu D, Yang C, Huang A, Dixon M, Hecht U. Intermetallics 2012;22:68–76.
[27] Gey N, Humbert M. Acta Mater 2002;50:277–87.
[28] Genç A, Banerjee R, Hill D, Fraser HL. Mater Lett 2006;60:859–63.
[29] Banerjee R, Genç A, Hill D, Collins PC, Fraser HL. Scr Mater 2005;53:1433–7.
[30] Hill D, Banerjee R, Huber D, Tiley J, Fraser HL. Scr Mater 2005;52:387–92.